Author/s:
Lyskov, I;Anda, A;Wong, YX;Tilley, AJ;Hall, CR;Thia, J;Russo, SP;Wong, WWH;Cole, JH;Smith, TA

Title:
Bilirubin analogues as model compounds for exciton coupling

Date:
2020-07-21

Citation:
Lyskov, I., Anda, A., Wong, Y. X., Tilley, A. J., Hall, C. R., Thia, J., Russo, S. P., Wong, W. W. H., Cole, J. H. & Smith, T. A. (2020). Bilirubin analogues as model compounds for exciton coupling. PHYSICAL CHEMISTRY CHEMICAL PHYSICS, 22 (27), pp.15567-15572. https://doi.org/10.1039/d0cp01421d.

Persistent Link:
https://hdl.handle.net/11343/344899

Journal Name

ARTICLE TYPE

Cite this: DOI: 00.0000/xxxxxxxxxx

Bilirubin analogues as model compounds for exciton coupling†

Igor Lyskov,[b,c] André Anda,[b,c] Yee X. Wong,[a,b] Andrew J. Tilley,[a,b] Christopher R. Hall,[a,b] Joel Thia,[a,b] Salvy P. Russo,[b,c] Wallace W. H. Wong,[a,b] Jared H. Cole[b,c] & Trevor A. Smith[a,b]

Received Date
Accepted Date

DOI: 00.0000/xxxxxxxxxx

A series of phycobilin analogues have been investigated to examine their potential for studies of coupled excitonic systems. These consist of a monomer, a tetrapyrrole structurally similar to bilirubin (bR), and two conjugated bR analogues. Spectroscopic and computational methods are used to investigate the degree of interchromophore coupling. We find the synthesized bR analogue shows stronger excitonic coupling than bR, owing to a different molecular geometry. The excitonic coupling in the conjugated molecules can be controlled by modifying the bridge side-group. New computed energy levels for bR using the DFT/MRCI method are also presented, which improve on published values and re-assign the character of excited singlet states.

The fate of electronic excitation energy following the absorption of light by large molecules is of importance in many photophysical processes. In photosynthetic systems, synthetic and bio-polymers, and in concentrated solutions and films, electronic excitation energy transfer can lead to the rapid relocation or delocalisation of excitation energy from the chromophore at which the initial excitation took place.[1] The strength of the coupling between moieties dictates the mechanism, rate and fate of the excitation energy reorganisation. Such processes have been investigated from both experimental and theoretical viewpoints, but these are often difficult to interpret and model in complex systems.

The simplicity of bichromophoric molecules makes them attractive targets to aid in determining the coupling between chromophores and the kinetics and mechanism of energy relocation within more complex multi-chromophoric systems. Bichromophoric molecules include bespoke systems in which the distance and orientation of the participating units are highly coordinated[2] through to common flexible fluorescent dyes[3,4]. Bilirubin (bR) and its chemical derivatives are tetrapyrroles (or phycobilins) that can be considered as an opened porphyrin ring forming a bichromophoric molecule (Figure 1-a) resulting in two non-conjugated dipyrrinone moieties, each with strongly allowed electronic transitions. The coupling between the two halves is weak but sufficient to allow the pair of chromophores to be modelled on the basis of fragment-localised Frenkel excitons[5,6]. Therefore, bR is of interest from the point of view of electronic excitation energy hopping mechanisms. Bilirubin is, of course, well-studied due to its involvement in the breakdown of haem in blood and related phototherapy of jaundice.

In order to study interactions between two halves of a bichromophore, a “model" or “half" molecule should be available for comparison. In studies of bR, semirubin[7] and xanthobilirubic acid (XBR) have been used as models.[8,9] However, since some of these model compounds can form dimers through intermolecular hydrogen bonds,[7] which is different to bilirubin’s intramolecular hydrogen bonding, and may isomerise,[10] these may not be ideal “half" bR models.

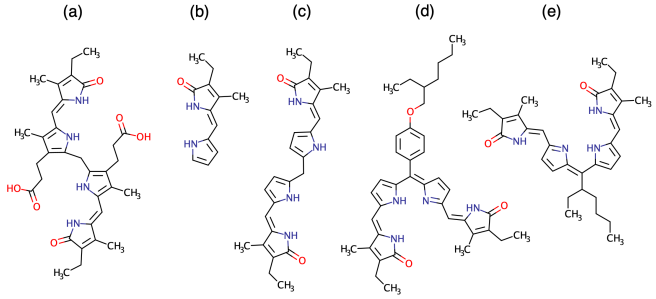

Fig. 1 Chemical structures of (a) bR and the phycobilin analogues studied: (b) monomer, (c) bR analogue, (d) conjugated dimer with aromatic side chain, (e) conjugated dimer

In this work we have designed and synthesised an analogue of bR (Figure 1-c) and its constituent monomer (Figure 1-b). We have also attempted to alter the electronic coupling between the

[a] School of Chemistry, University of Melbourne, Parkville, Australia. E-mail: trevoras@unimelb.edu.au
[b] ARC Centre of Excellence in Exciton Science
[c] Chemical and Quantum Physics, School of Science, RMIT University, Melbourne, Australia

† Electronic Supplementary Information (ESI) available: See DOI: 00.0000/00000000.

two halves by including a conjugated link between them. This required a side chain to provide solubility, and two versions of the conjugated dimer have been investigated (Figure 1-d,e). Variation of the side chain provides another strategy to alter the interactions between the two halves. These molecules have been studied by means of quantum chemistry and by UV/vis absorption spectroscopy.

The non-conjugated phycobilin derivative (Figure 1-c) was synthesized by Knoevenagel condensation between 5,5'-methylenebis(1H-pyrrole-2-carbaldehyde) [11] and four equivalents of commercially available 3-ethyl-4-methyl-1,5-dihydropyrrol-2-one [12] (Figure 1-b). Purification by precipitation of the reaction mixture into excess water gave the non-conjugated phycobilin in 74% yield. Synthesis of the conjugated phycobilin analogues (Figure 1-d,e) began with Knoevenagel condensation between pyrrole-2-carboxaldehyde and two equivalents of 3-ethyl-4-methyl-1,5-dihydro-pyrrol-2-one to give molecule **b** in near-quantitative yield. Lewis acid-mediated condensation between the desired aldehyde and two equivalents of bis-pyrrole, followed by DDQ oxidation, afforded the conjugated phycobilin derivatives, with purification achieved by column chromatography on basic alumina.

The absorption spectra were recorded using a UV-Vis spectrophotometer (Varian Cary 50). The samples were dissolved in spectroscopic grade ethanol and diluted to an optical density of 0.1 for a 10 mm path length cuvette. A reference measurement on pure ethanol solution was made for background subtraction. To understand the origin of the absorption signals we carried out a series of quantum-chemical calculations. The ground state geometry of the molecules was optimized using density functional theory (DFT) with the Perdew-Burke-Ernzerhof (PBE) exchange-correlation functional [13] including D3-BJ dispersion correction [14,15] as implemented in the TURBOMOLE package [16]. The split valence triple-ζ basis set TZVP [17] was utilized for all atoms. The excited-state properties were computed with the hybrid semiempirical DFT/MRCI-R2016 method [18] in conjunction with the TZVP atomic basis set. The environmental effects of ethanol were modelled using the continuum solvation model COSMO [19].

The calculated and recorded optical absorption spectra of the five compounds under investigation in ethanol are shown in Figure 2. The absorption of the monomer (Figure 2-b) peaks at 381 nm, which is at higher energy than the absorption spectrum reported for XBR. [8,9]. This strong $\pi\pi^*$ transition originates mainly from promoting an electron from the highest occupied molecular orbital (HOMO) to the lowest unoccupied molecular orbital (LUMO). The absorption of bR in ethanol (Figure 2-a) peaks at 451 nm with a broad shoulder centered at about 425 nm. The DFT/MRCI calculations reveal that the first two excited singlets S_1 and S_2, which are red-shifted by 0.22 eV compared to the experiment, are responsible for these features. Contrary to the B3LYP results of Granucci *et.al.* [6], which predict the two lowest singlet states possess charge-transfer character, we assign S_1 and S_2 to localised Frenkel types. This difference is attributed to well-known drawbacks of hybrid functionals for describing the long-range interparticle potential [20]. The non-zero interaction between

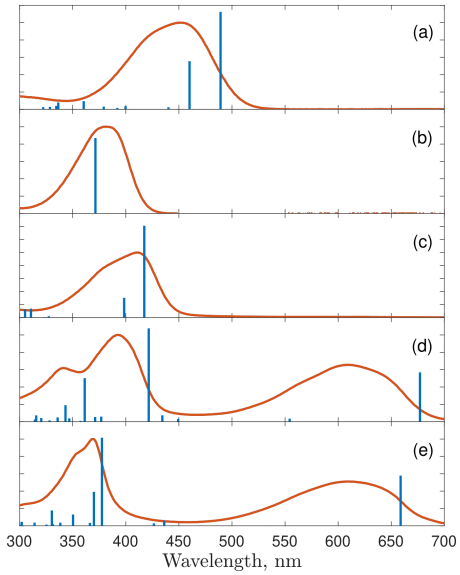

Fig. 2 UV-visible absorption spectra of systems studied: (a) bR, (b) monomer, (c) bR analogue, (d) conjugated dimer with aromatic side chain, (e) conjugated dimer with 2-ethylhexyl side chain. Calculated electronic transitions are shown with blue bars

the localised excitons enables configuration mixing, hence, redistributing the overall oscillator strength.

The spectrum of the bR analogue (Figure 2-c) closely matches that for bR itself but is blue-shifted to 411 nm and 380 nm. Similar to bR, the underlying S_1 and S_2 transitions are formally given by an interplay of HOMO,HOMO-1 and LUMO,LUMO+1 orbitals. The DFT/MRCI wavelength of 417 nm and 398 nm for the most prominent bands agree very well with experiment. The absorption peak of the monomer (**b**) occurs at higher energy than the bR analogue (**c**), which is also the case for bR/XBR. The differences between the absorption spectra of the model and the dimer, in both bR/XBR and **b**/**c** cases, indicate the occurrence of ground-state interactions between the two chromophores in the corresponding dimer.

In contrast to the other compounds, the absorption spectra of both the two conjugated dimer molecules (Figure 2-d,e) show an additional strong absorption band, significantly to the red of the other peaks, centered at 608 nm. This is reconciled on the basis of the extended conjugation between the two halves of the dimer that is not present in the bilirubin analogue. In addition to this, both molecules have two absorption bands in the UV region with the highest intensity peak at 393 nm for system **d** and slightly shifted to 369 nm for system **e**. In spite of almost identical spatial orientation and distance between the two bis-pyrrole halves, both the DFT/MRCI and experimental absorption spectra display substantially different fine splitting between the two peaks. This compels us to consider the influence of a side chain on the excited-state structure as a potential explanation of this difference. Because the multiconfigurational character of the optically active states hinders the wavefunction analysis for perceptible traces of the interchromophore linker, we have computed the S_0-S_x density difference caused by excitation to the bright

S_x states (Figure 3). In contrast to the S_1 where the exciton is predominantly delocalised over the bis-pyrrole halves, the most prominent UV S_5 and S_8 transitions in molecule **d** are affected by the phenol ring of the side chain. In both cases we found a reduction of electron density on the aromatic ring implying that it acts as an electron-donating unit in the excited state.

To further understand the role of the side chain we performed charge-transfer (CT) analysis based on the one-particle transition density matrix. This provides the percentage of Frenkel and CT character in the underlying wavefunction of an electronically excited state[21]. We schematically divide the molecule **d** into two subsystems consisting of a conjugated pair of monomers (subsystem B) and a residual aromatic side chain (subsystem A) as illustrated in Figure 3-c. Thereby we aim to compute the configurational weight of an electron transfer from subsystem A to subsystem B via the S_5 and S_8 excitations. The reduced one-particle transition density matrix n_{ij} for an arbitrary $S_0 \rightarrow S_x$ transition in the molecular orbital (MO) basis is given by:

$$n_{ij}^{0x} = \sum_{\sigma} \langle \psi_0 | \hat{a}_{j\sigma}^{\dagger} \hat{a}_{i\sigma} | \psi_x \rangle \tag{1}$$

where σ is electronic spin index, $\hat{a}^{\dagger}$ and $\hat{a}$ are creation and annihilation operators of the Fermi type. The matrix n^{0x} can be expressed in the atomic orbital (AO) basis through the elements of the MO expansion coefficients $c_{\mu i}$ as:

$$\tilde{n}_{\mu\nu}^{0x} = \sum_{ij} c_{\mu i} n_{ij}^{0x} c_{\nu j} \tag{2}$$

By taking into account the overlap matrix S between the AOs to ensure orthonormality, the charge-transfer matrix elements can be computed through

$$\omega_{AB} = \frac{1}{2} \sum_{\mu \in A} \sum_{\nu \in B} (\tilde{n}^{0x} S)_{\mu\nu} (S\tilde{n}^{0x})_{\mu\nu} \tag{3}$$

where orbitals μ and ν are localized on the atoms of subsystem A and B, respectively. This analysis reveals that the brightest S_5 state exhibits 45% of CT character, that is, an electron transfer from the phenol ring to the bis-pyrrole units. The admixture of the charge-transfer contribution in the wavefunction significantly stabilises the S_5 energy in system **d** compared to that in system **e**, where the aromatic ring is not present. To a somewhat lesser extent the S_8 state is affected, which revealed 22% of the electron-transfer component. The remaining part of the wavefunction is ascribed to the neutral Frenkel exciton residing on subsystem B. We did not find evidence of a long-wavelength transition (>300 nm) situated on subsystem A.

Overall, the DFT/MRCI method accurately reproduces the UV-vis measurements for molecules **b,c,e**, and slightly underestimates the energy of states of **a,d** by not more than 0.2 eV. The latter energy shift is applied more or less consistently for all of the peaks, so that it changes the spectral onset while the splitting between energy levels is maintained as in the UV/vis measurements.

As the absorption spectra of all compounds can be simulated adequately we have attempted to compute the excitonic coupling

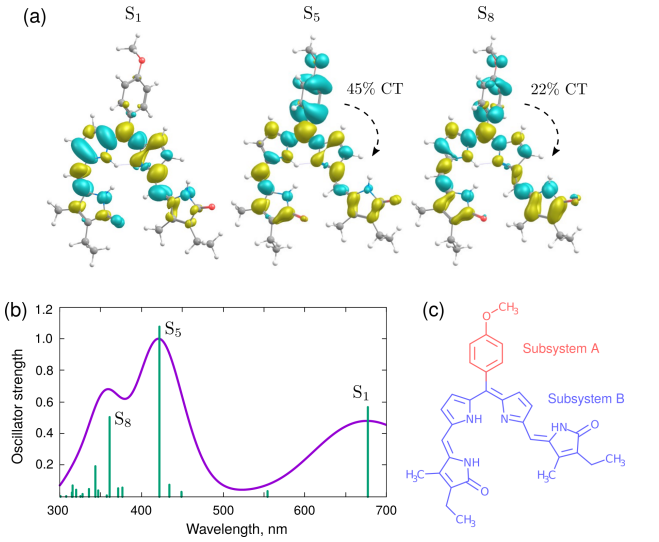

Fig. 3 (a) The electronic density difference originating from the $S_0 \rightarrow S_x$ excitation. A density loss/gain is painted in green/yellow. (b) The DFT/MRCI spectrum for molecule **d** convoluted with gaussians of 1500 cm^{-1} width. (c) Partitioning of system **d** into two subsystems.

between the moieties. The excitonic coupling between the two covalently linked halves of bR and the bR analogue (molecules **a** and **c**) can, in the absence of hydrogen bonding, be evaluated using the monomer transition density (MTD) approach[21,22]. In the following let ψ_α and ψ_{α^*} denote the wave function of the ground and electronically excited states localized on the first fragment, respectively, and ψ_β and ψ_{β^*} are on the second fragment. Then, the electronic interaction between two singlet excited states $\alpha^*\beta$ and $\alpha\beta^*$, which are perfectly localized on respective subsystems, can be evaluated as:

$$\langle \psi_{\alpha^*} \psi_\beta | \psi_\alpha \psi_{\beta^*} \rangle = \sum_{ij} \sum_{kl} n_{ij}^{\alpha\alpha^*} n_{kl}^{\beta\beta^*} \left[(ij|kl) - \frac{1}{2}(il|kj) \right] = J - K \tag{4}$$

where the Mulliken convention for two-particle integrals is utilized:

$$(ij|kl) = \int \frac{d\vec{r}_1 d\vec{r}_2}{|\vec{r}_1 - \vec{r}_2|} \phi_i^{\dagger}(\vec{r}_1) \phi_j(\vec{r}_1) \phi_k^{\dagger}(\vec{r}_2) \phi_l(\vec{r}_2) \tag{5}$$

The electronic coupling in Eq. 4 is given by a combination of Coulomb (J) and exchange (K) contributions, which are known to mediate the Förster and Dexter couplings. The repulsion integrals over MOs in Eq. 5 are evaluated using the resolution-of-identity (RI) approach:

$$(ij|kl) \approx \sum_{P} b_{ij}^{P} b_{kl}^{P} \tag{6}$$

with

$$b_{ij}^{P} = \sum_{Q} (ij|Q) V_{PQ}^{-1/2}. \tag{7}$$

Here, P and Q label the auxiliary basis function and $V_{PQ}^{-1/2}$ is an element of the inverse square root metric matrix $V_{PQ} = \int d\vec{r}_1 d\vec{r}_2 P(\vec{r}_1) Q(\vec{r}_2) / r_{12}$.

The MTD calculations were based on the DFT/MRCI transition density matrix constructed for the individual S_1 states of the constituent fragments of a dimer at the optimized geometry (Table 1). The computed interfragment couplings for bilirubin and its non-conjugated analogue are almost exclusively composed of the Coulumb contribution and are 687 cm^{-1} and 1021 cm^{-1}, respectively. The origin of this difference can be qualitatively understood in the framework of the so-called ideal dipole approximation (IDA), which ignores the Dexter term and approximates the Förster term by a classical interaction of individual transition dipoles moments $\vec{d}$:

$$\langle \psi_{\alpha^*}\psi_\beta | \psi_\alpha \psi_{\beta^*} \rangle \approx \frac{\vec{d}_\alpha \vec{d}_\beta}{\vec{R}^3} - 3\frac{(\vec{d}_\alpha \vec{R})(\vec{d}_\beta \vec{R})}{\vec{R}^5} \quad (8)$$

In contrast to the non-conjugated bR analogue, the monomers in bR are held together by an intramolecular network of hydrogen bonds[23], which overall arrange the moieties in perpendicular planes.[9] By taking the interchromophore distance $\vec{R}$ as a radius connecting the gravity centers of the monomers, the IDA yields coupling of 355 cm^{-1} for system **a** and 514 cm^{-1} for system **c**. Note, that the Mulliken population analysis based on DFT-B3LYP calculations of Granucci *et. al*[6] yields a 0.11 eV coupling constant for bilirubin. This is slightly stronger than our value, which is likely to be a factor of both choices of the electronic structure method and the diabatization scheme. Although the coupling magnitude is substantially different in the IDA and MTD calculations, both approaches draw similar trends in that coupling in bilirubin is weaker than in the non-conjugated dimer (**c**). The discrepancy between the methods is due to the inaccuracy of IDA when R is of the same order as a molecular radius. Nonetheless, this suggests that mutual orientation of fragments in space is a reason for stronger excitonic coupling in non-conjugated bilirubin analogue.

Table 1 Coulomb (J) and exchange (K) components of excitonic coupling matrix elements for all bichromophoric systems from Figure 1

	J, cm^{-1}	K, cm^{-1}	J-K, cm^{-1}
system **a**	700	13	687
system **c**	1035	14	1021
system **d**			≈4500
system **e**			≈5700

The MTD formalism goes beyond the four electrons/four orbitals model, as it takes into account all electronic configurations spawned by single excitation operators. However, the ionic contributions of $\alpha^-\beta^+$ and $\alpha^+\beta^-$ types cannot be captured by the transition density of monomers. This becomes critical when frontier MOs are delocalized over both monomers, which is the case in conjugated dimers. As a consequence of this, the wavefunctions of the excited-states inevitably inherit significant charge-transfer configurations making the monomer-exciton basis insufficient for evaluating the couplings. In this case we can estimate the interfragment coupling V by the energy difference between the two optically bright states $\Delta E = 2V$, which returns ≈4500 cm^{-1} for system **d** and ≈5700 cm^{-1} for system **e**. The resulting excitonic couplings in the conjugated dimers are much stronger than in their non-conjugated counterparts. Such a strong interchromophore interaction is a result of two rigidly bound π-conjugation monomers, which in fact cannot be viewed as two separated excitonic systems.

In summary, we have synthesized conjugated and nonconjugated bichromophoric phycobilin analogues and explored their electronically excited states with UV-vis spectroscopy and electronic structure methods. The DFT/MRCI reproduces fairly well the main peaks in electronic absorption spectra and provides a balanced description of the signal intensities. Following the conventional Förster theory, the mutual orientation of half-molecules controls the interfragment excitonic coupling in nonconjugated systems. At the same time, the coupling magnitude in π-conjugated molecules can be effectively controlled by altering the side chain off the link connecting the two moieties.

Conflicts of interest

There are no conflicts to declare.

Acknowledgements

This work was supported by the Australian Government through the Australian Research Council (ARC) under the Centre of Excellence scheme (project number CE170100026). It was also supported by computational resources provided by the Australian Government through the National Computational Infrastructure National Facility and the Pawsey Supercomputer Centre.

Notes and references

1 V. I. Novoderezhkin and R. van Grondelle, *Phys. Chem. Chem. Phys.*, 2010, **12**, 7352–7365.
2 G. D. Scholes, K. P. Ghiggino, A. M. Oliver and M. N. Paddon-Row, *J. Am. Chem. Soc.*, 1993, **115**, 4345–4349.
3 Y. H. Lee, S. Park, J. Oh, J. W. Shin, J. Jung, S. Yoo and M. H. Lee, *ACS Appl. Mater. Interfaces*, 2017, **9**, 24035–24042.
4 N. A. Kukhta, A. S. Batsanov, M. R. Bryce and A. P. Monkman, *J. Phys. Chem. C*, 2018, **122**, 28564–28575.
5 G. J. Troup, G. Agati, F. Fusi and R. Pratesi, *Aust. J. Phys.*, 1996, **49**, 673–682.
6 G. Granucci, M. Mazzoni, M. Persico and A. Toniolo, *Phys. Chem. Chem. Phys.*, 2005, **7**, 2594–2598.
7 M. T. Huggins and D. A. Lightner, *The Journal of Organic Chemistry*, 2000, **65**, 6001–6008.
8 D. A. Lightner, M. Reisinger and G. L. Landen, *J. Biolog. Chem.*, 1986, **261**, 6034–6038.
9 M. Mazzoni, G. Agati, G. J. Troup and R. Pratesi, *J. Opt. A: Pure Appl. Opt.*, 2003, **5**, S374–S380.
10 B. Zietz and F. Blomgren, *Chemical Physics Letters*, 2006, **420**, 556–561.
11 J. Ostapko, K. Nawara, M. Kijak, J. Buczyńska, B. Leśniewska, M. Pietrzak, G. Orzanowska and J. Waluk, *Chem. Eur. J.*, 2016, **22**, 17311–17320.
12 L. L. Chepelev, C. S. Beshara, P. D. MacLean, G. L. Hatfield, A. A. Rand, A. Thompson, J. S. Wright and L. R. C. Barclay, *J. Org. Chem.*, 2006, **71**, 22–30.
13 J. P. Perdew, K. Burke and M. Ernzerhof, *Phys. Rev. Lett.*, 1996, **77**, 3865–3868.
14 S. Grimme, J. Antony, S. Ehrlich and H. Krieg, *J. Chem. Phys.*, 2010, **132**, 154104.
15 S. Grimme, S. Ehrlich and L. Goerigk, *J. Comput. Chem.*, 2011, **32**, 1456–1465.
16 *TURBOMOLE v7.2 2017, a development of University of Karlsruhe and Forschungszentrum Karlsruhe GmbH, 1989-2007, TURBOMOLE GmbH, since 2007; available from* `http://www.turbomole.com`.
17 A. Schäfer, C. Huber and R. Ahlrichs, *J. Chem. Phys.*, 1994, **100**, 5829–5835.
18 I. Lyskov, M. Kleinschmidt and C. M. Marian, *J. Chem. Phys.*, 2016, **144**, 034104.
19 A. Klamt and G. Schüürmann, *J. Chem. Soc., Perkin Trans. 2*, 1993, **5**, 799–805.
20 A. Dreuw and M. Head-Gordon, *J. Am. Chem. Soc.*, 2004, **126**, 4007–4016.
21 J. D. Spiegel, I. Lyskov, M. Kleinschmidt and C. M. Marian, *Chem. Phys.*, 2017, **482**, 265–276.
22 R. F. Fink, J. Pfister, A. Schneider, H. Zhao and B. Engels, *Chem. Phys.*, 2008, **343**, 353–361.
23 R. Bonnett, J. E. Davies, M. B. Hursthouse, G. M. Sheldrick and D. M. C. Hodgkin, *Proc. R. Soc. Lond. B*, 1978, **202**, 249–268.